LAWRENCE
LIVERMORE
NATIONAL
LABORATORY

LLNL-JRNL-455938

# Electronic Structure of Warm Dense Copper Studied by Ultrafast X-ray Absorption Spectroscopy

B. I. Cho, K. Engelhorn, A. A. Correa, T. Ogitsu, C. P. Weber, H. J. Lee, J. Feng, Y. Ping, A. J. Nelson, R. W. Lee, R. W. Falcone, P. A. Heimann

September 20, 2010

Physical Review Letters

## Disclaimer

# Electronic Structure of Warm Dense Copper Studied by Ultrafast X-ray Absorption Spectroscopy

B. I. Cho,[1] K. Engelhorn,[1,2] A. A. Correa,[3] T. Ogitsu,[3] C. P. Weber,[4] H. J. Lee,[5] J. Feng,[1]

Y. Ping,[3] A. J. Nelson,[3] D. Prendergast,[6] R. W. Lee,[3] R. W. Falcone[1,2,7] and P. A. Heimann[1]

[1]*Advanced Light Source, Lawrence Berkeley National Laboratory, Berkeley, CA 94720*

[2]*Applied Science and Technology, University of California, Berkeley, CA 94720*

[3]*Lawrence Livermore National Laboratory, Livermore, CA 94550*

[4]*Department of Physics, Santa Clara University, Santa Clara, CA 95053*

[5]*Linac Coherent Light Source, SLAC National Accelerator Laboratory, Menlo Park, CA 94025*

[6]*Molecular Foundry, Lawrence Berkeley National Laboratory, Berkeley, CA 94720*

[7]*Department of Physics, University of California, Berkeley, CA 94720*

**Abstract**

We use time-resolved x-ray absorption spectroscopy to investigate the unoccupied electronic density of states of warm dense copper that is produced isochorically through the absorption of an ultrafast optical pulse. The temperature of the superheated electron-hole plasma, which ranges from 4000 to 10000 K, was determined by comparing the measured x-ray absorption spectrum with a simulation. The electronic structure of warm dense copper is adequately described with the high temperature electronic density of state calculated by the density functional theory. The dynamics of the electron temperature are consistent with a two-temperature model, while a temperature-dependent electron-phonon coupling parameter is necessary.

Understanding the properties of warm dense matter (WDM) is a research area that has attracted much interest recently [1-5]. The WDM regime falls in between condensed matter and plasmas, where it is defined by a temperature of ~ $10^4$ K (~ 1 eV) and near solid densities. Matter in this extreme condition is ionized, but its theoretical description is quite different from both traditional plasma and/or condensed matter physics, because the thermal energy is close to the Fermi energy and the ion-ion coupling parameter is an order of unity [6]. Nonetheless, studying this superheated solid or strongly coupled plasma can provide key understandings about non-equilibrium phase transitions and energy relaxation processes, which are critical to model many phenomena found in astrophysics [7], inertial confinement fusion [8], as well as the applied processes of laser machining and ablation [9].

From the experimental point of view, creating WDM and maintaining such high temperature and pressure conditions in the laboratory causes many difficulties. For quantitative WDM studies one should specify the location in the phase diagram, which necessitates the measurement of two of the three state variables: temperature, density and pressure. By using a femtosecond optical laser pulse which is absorbed by electrons near the surface and matching a sample thickness to the length scale of ballistic electron transport, isochoric heating across the sample with a known density is obtained [1]. On the other hand, the temperature and pressure are difficult to measure. For the measurement of temperature, optical pyrometry signal levels will be low and the emissivity must be assume. Although x-ray Thomson scattering has demonstrated the capability to determine the temperature in addition to the electron density and ionization degree [2], at present Thomson scattering has a temperature uncertainty that will be relatively large for these low temperatures, making it more suitable to temperatures > 10 eV.

As warm dense matter states are predominantly non-equilibrium, ultrafast techniques are essential to probe the transient (~ ps) material properties. In this way the optical properties of warm dense gold have been successfully investigated [3]. However, because of the near solid density of WDM, the probing depth with optical lasers is limited. From optical data it is also difficult to access direct information on atomic structure. X-ray techniques, especially based upon synchrotron radiation, provide a powerful tool for the study of materials. In particular, x-ray absorption spectroscopy provides information on electronic structure and optical pump / x-ray probe techniques have been developed to study dynamical properties [10]. Recently, a study of x-ray absorption spectrum (XAS) of warm dense aluminum heated by laser-accelerated protons was reported [4]. There a broadening of the *K* edge was observed that was caused first by the change in the electron population near the Fermi energy associated with the high temperature. In addition, they interpreted a loss of structure in the absorption spectrum as resulting from a loss of order in the high temperature liquid. For copper, a photoemission study using ultrafast laser-heating observed a reduced intensity in the *3d* peak. This change was interpreted as caused by a lower occupation of the *d* band at the elevated electron temperature [5].

Here we present a study of the electronic structure of warm dense copper created by ultrafast laser excitation and probed by time resolved x-ray absorption spectroscopy. The x-ray absorption spectrum near the copper *L* edges probes the unoccupied electronic density of states (DOS) in 3*d* and 4*s* bands according to the dipole selection rule. Under strong optical excitation, solid density copper with energy density of $3.6 \times 10^6$ J/kg is created, and its electron temperature is quickly increased to ~ 1 eV. The experimental XAS was compared with the theoretical one derived from first-principles Density Functional Theory (DFT) simulations. We compare the

measured and simulated x-ray absorption spectra to determine electron temperature of the superheated electron-hole plasma in the ~ $10^4$ K regime. The time dependence of electron temperature allows us to study the electron-phonon coupling of the non-equilibrium state of warm dense copper.

The experiment was performed at beamline 6.0.2 of the Advanced Light Source (ALS) synchrotron radiation facility. The laser pump and x-ray probe setup is depicted in Fig 1. A Ti:sapphire laser pulse with duration of 150 fs is split into three paths. The first pulse is frequency doubled to a wavelength of 400 nm and focused (250 × 200 $\mu$m FWHM) onto the foil with the fluence of up to 0.5 J/cm$^2$ to isochorically heat the copper sample. The second pulse triggers the photoconductive switch of the x-ray streak camera. The third is frequency tripled and split to generate two timing fiducials separated in time by 6.7 ps and imaged along with an x-ray pulse. The sample is composed of a freestanding copper foil of 70 nm thickness coated on both sides with 6 nm of amorphous carbon to prevent oxidation of the copper. A measurement of the reflection and transmission of the 400 nm laser light indicates that 60% of the laser energy is absorbed in the sample. The experiments are performed at the laser fluence above the damage threshold, therefore the sample is translated to the fresh location after each laser shot.

The probe is provided by broadband, 70 ps pulse duration x-rays from an ALS undulator tuned to the copper *L* edges at 933 and 952 eV. The x-ray bandwidth and the imaging of the streak camera allow the entire X-ray Absorption Near-Edge Structure (XANES) to be detected for each x-ray pulse. The x-ray spot size was set to 200 × 150 $\mu$m for the spatial overlap with the laser focus. X-rays transmitted through the sample enter a Variable-Line-Spacing (VLS) grating spectrometer, which provides an energy resolution of 1.1 eV at the copper *L* edges [11]. Dispersed x-rays enter the streak camera, which has a temporal resolution of 2 ps. This streak

camera detector provides 2-dimensional images of the x-ray pulse with time on one axis and photon energy on the other [12].

The 400 nm photons are absorbed by the 3*d*-4*p* interband transition and create a superheated electron-hole plasma in *d* and *s*/*p* bands. This absorption process occurs near the front surface of the sample because of the 14 nm optical penetration depth in copper [13]. However, the ballistic motion of excited electrons with velocity close to the Fermi velocity, ~ $10^6$ m/s, delivers energy into the deeper part of the sample and the isothermal condition across the sample is approximately achieved since the sample thickness is set to the mean free path of electrons in solid copper, 70 nm [14]. Fourier Domain Interferometry (FDI) of copper at a similar laser fluence indicates that the uniformity of energy density across the sample is maintained within a factor of two [15]. Following the ultrafast laser pulse a constant density will be maintained by material strength and inertia for time of order 1 ps [1].

Figure 2(a) shows the streaked x-ray transmission image of warm dense copper for which 150 images were averaged. The sample is irradiated with an incident laser fluence of 0.33 ± 0.07 J/cm$^2$. The laser pulse at $t = 0$ introduces a rapid increase in the absorption, *i.e.*, a decrease in the transmission, below both the $L_2$ and $L_3$ edges that slowly recovers in ~ 20 ps. At negative time, the room temperature transmission is observed. Using this data, the time and energy resolved x-ray absorption cross-section $\sigma(E,t)$ can be derived from $\sigma = \ln(I_0/I)/(\rho l)$, where $\rho$ and $l$ are the density and thickness of the sample, and $I_0$ and $I$ are the incident and transmitted x-ray intensities.

Figure 2(b) exhibits the XAS of warm dense copper at selected times. The initially deposited energy density is 3.6 ± 0.7 × $10^6$ J/kg. After 6 ps changes in the absorption spectrum are more gradual, and as a result an increased time step is chosen. The room temperature

spectrum is averaged over 70 ps and consequently has better signal-to-noise (S/N) than the individual WDM absorption spectra. The three peaks of XANES spectrum follow the observed solid copper spectrum under ambient conditions [16]. Because of the 2 ps streak camera time resolution, the XAS at $t = 0$ includes an average of the WDM spectra and the room temperature spectrum. At 2 ps, the position of the $L_3$ edge is shifted by 3 eV to lower photon energy, and the absorption above the original $L_3$ edge is decreased by ~ 10%. Around the $L_2$ edge, the same phenomena are observed although the effects are smaller because of the larger $L_2$ natural linewidth caused by the allowed Coster-Kronig Auger transition [17]. Similar changes are seen in the 4 ps spectrum, but after 6 ps, the $L_3$ edge appears broadened, and by 20 ps time delay the difference from the room temperature XAS is further reduced. These dynamics indicate that electrons are excited from below to above the Fermi level $E_F$, and that there is a relaxation of the electronic excitation on a time scale of ~ 6 ps.

To further interpret the measured XAS, it is necessary to compare with simulations. At high temperatures, liquid atomic configurations are generated using first-principles Density Functional Theory (DFT) molecular dynamics (MD) simulations. For the initial state, a face centered cubic solid at ambient conditions is assumed. For all of our simulations, an ultrasoft pseudopotential is used to describe the copper ions with *3d*, *4s* and *4p* as valence states, and the electronic wavefunctions are expanded by a planewave basis. A cubic supercell containing 32 copper atoms is used. The electronic structure is optimized for each time step and the atomic configuration is propagated based on Newtonian equation. For the MD simulations, the Chadi-Cohen's two special k-points sampling for fcc crystal was used. On those atomic configurations, the x-ray absorption cross sections are calculated from the dipole transition matrix elements between the Cu *2p* core state and unoccupied states (Kohn-Sham eigenstates). The Quantum

Espresso package [18] is used to generate both the atomic configurations and the Kohn-Sham eigenstates, and the prescription developed by Prendergast and Galli is used to reconstruct the oscillatory property of electronic wavefunctions near the vicinity of nuclei from the smoothed pseudo wavefunctions [19]. The k-points integration is performed using the interpolation scheme described in Ref [20] so as to achieve a good numerical convergence of the spectrum ($16^3$ k-points grid after the interpolation).

First, the XAS at the room temperature is calculated [Figure 3(a)]. The Fermi distribution for 300 K is applied to the solid x-ray absorption cross section. The total x-ray absorption spectrum, $L_{2,3}$, is constructed as the superposition of $L_2$ and $L_3$ edges, where the $L_2$ edge is obtained by shifting $L_3$ edge spectrum by 20 eV. The $L_3$:$L_2$ branching ratio of 1.8:1 is chosen to fit the experimental spectra. We note that deviations from the statistical 2:1 ratio of $L_3$:$L_2$ is observed for *3d* transition metals [21]. A single scaling factor adjusted the absolute cross section of the calculations to the measurements. Energy and the edge dependent lifetime broadening is separately added to the $L_3$ and $L_2$ edge spectra [22]. The whole spectrum is convolved with a 1.1 eV Lorentzian function, representing the experimental resolution.

For the XAS of warm dense matter, the x-ray absorption cross section is calculated for high temperature liquid Cu. Initially the optical excitation heats the electrons and the ions remain cold. However, on a timescale less than the detector resolution, the electron-phonon coupling may increase lattice temperature higher than the melting temperature. The high temperature XAS are calculated by again applying a Fermi-Dirac distribution, because the hot electrons are expected to quickly thermalize on a timescale less than the streak camera resolution [23].

Typical comparisons of the measured and calculated XAS are shown in the Fig 3(b,c). Because of the sensitivity of the *L*-edges to the electron temperature, at each time step of the

evolving warm dense matter state, the electron temperature can be determined with an accuracy of ~ 1000 K by comparing the edge shift and broadening. It is noted that the chemical potential $\mu$ shifts to higher energy as the temperature increases because of the high DOS below the Fermi level. From the conservation of the total number of electron $N_e$, the chemical potential can be obtained by $N_e = \int_{-\infty}^{\infty} f(E,\mu,T_e)g(E)dE$, where $g$ is the electron DOS. The strong red shift of the *L*-edge at early time is a consequence of the elevated electron temperature and the high *d*-DOS below the Fermi level. The broadening of the edge at later times (e.g. 9 ps) results from the lower electron temperatures. It is also noted that the calculated XAS reproduces the shape of the experimental XAS above the edge (932 ~ 945 eV), which has ~ 10 % lower absorption than the room temperature solid. This reduced absorption cannot be explained by the electron occupation at ~ 10000 K. The solid and liquid DOS at these energies are also similar [Fig 3(d)]. Therefore, the change in the XAS above the edge must be explained by a decrease in the x-ray absorption matrix elements for the $2p \rightarrow s, d$ transitions. Overall, there is a quantitative agreement between the measured and calculated XAS.

We note that the electron temperature of copper determined by comparing experimental and calculated XAS is sensitive to the energy of the *d*-band. In fact, the calculated energy of the *d*-band of solid copper is overestimated by 0.4 eV when referred to photoemission spectroscopy data and the overestimation of the *d*-band energy is a common disadvantage of the DFT methods [24].

The dynamical evolution of the electron temperature is shown in the Fig. 4. At the energy density of $3.6 \pm 0.7 \times 10^6$ J/kg, the measured electron temperature quickly increases to a peak of ~ 10200 K at 2 ps. It starts to decrease and reaches ~ 4500 K after 10 ps. To understand the observed dynamics of warm dense copper, we employ the two-temperature model (TTM) [25].

This model, widely used to describe femtosecond laser-solid interactions, separates the electrons and lattice into two sub-systems, and describes the temporal evolution of the electron and lattice temperatures ($T_e$ and $T_l$) with two non-linear equations.

$$C_e(T_e)\frac{dT_e(t)}{dt} = -G(T_e)\left[T_e(t) - T_l(t)\right] + S_L(t)$$
$$C_l\frac{dT_l(t)}{dt} = G(T_e)\left[T_e(t) - T_l(t)\right]$$

Here $G$ is the electron-phonon coupling factor, while $C_e$ and $C_l$ are the electron and lattice heat capacities, respectively. $S_L$ is the energy deposition by the laser pulse, given by $\Delta\varepsilon\varrho_{Cu}/(t_0\sqrt{\pi})$ $\exp[-t^2/t_0^2]$ where $t_0 = 90$ fs.

The electron heat capacity is obtained from the derivative of the Fermi-Dirac distribution with respect to temperature the lattice heat capacity, $C_l = 3.5 \times 10^6$ J/m$^3$K, is obtained by the Dulong-Petit law and is assumed to be constant.

For the electron-phonon coupling parameter, a value of $G_0 = 10^{17}$ Wm$^{-3}$ K$^{-1}$ is experimentally measured up to the temperature of 2200 K [26]. Recently, Lin *et al*. derive an expression for the electron temperature-dependent electron-phonon coupling factor $G(T_e)$ and calculate the values for various metals including copper [27].

Using the calculated $C_e(T_e)$ and the values of $G(T_e)$ from the Ref. [27], $T_e(t)$ and $T_l(t)$ have been derived. The same calculations with a constant $G_0$ have also been performed for comparison. The results are shown in Fig. 4 for an energy density of $3.6 \times 10^6$ J/kg. To account for the streak camera time resolution, each curve is convoluted with a Lorentzian function having 2 ps FWHM.

Both results show that the electron temperature peaks at the end of the laser pulse, and then the electron temperature decreases. But comparing to the constant $G_0$, the $T_e$-dependent electron-phonon coupling parameter $G(T_e)$ provides lower values of electron temperature, a

faster decrease in $T_e$, and as a result a better agreement with the experimental data. It indicates that the electron-phonon coupling factor of copper is enhanced in this temperature regime.

We note that at longer time delay the experimentally-observed electron temperatures are lower than the TTM calculations, indicating the onset of additional electron cooling mechanisms. In fact, hydrodynamic motion, which for a similar energy density in copper has a time scale of ~ 5 ps [15], consistent with the temperature reduction.

In conclusion, we have observed the evolution of the unoccupied electron DOS of warm dense copper via time-resolved XAS. Good agreement is observed between measured x-ray absorption spectra and calculated spectra, based on the DOS of liquid copper. From the edge shift and broadening, the electron temperature of non-equilibrium states of warm dense matter could be determined in the 10000 K regime. The reduction of x-ray absorption above the edge results from a change in the transition matrix elements. The evolution of electron temperature can be described by a two-temperature model including a $T_e$-dependent electron heat capacity and electron-phonon coupling factor.

We authors would like to acknowledge stimulating discussions with E. Henestroza and A. Ng. These experiments were carried out at the Advanced Light Source, supported by the Director, Office of Science, Office of Basic Energy Sciences, Materials Sciences Division, of the U.S. Department of Energy under Contract No. DEAC03-76SF00098 at Lawrence Berkeley National Laboratory and a part of the work was performed by Lawrence Livermore National Laboratory under Contract DEAC52-07NA27344 and the LDRD program at LLNL (08-ERD-005).

**References**


[1] A. Forsman *et al*., Physical Review E **58**, R1248 (1998).

[2] H. J. Lee *et al*., Physical Review Letters **102**, 115001 (2009).

[3] Y. Ping *et al*., Physical Review Letters **96**, 255003 (2006).

[4] A. Mančić *et al*., Physical Review Letters **104**, 35002 (2010).

[5] A. Nelson *et al*., Applied Physics Letters **87**, 154102 (2005).

[6] S. Ichimaru, Reviews of Modern Physics **54**, 1017 (1982).

[7] M. Ross, Nature **292**, 435 (1981).

[8] M. Koenig *et al*., Applied Physics Letters **72**, 1033 (1998).

[9] J. W. Chan *et al*., Optics Letters **26**, 1726 (2001).

[10] S. Johnson *et al*., Physical Review Letters **91** (2003).

[11] P. A. Heimann *et al*., AIP Conference Proceedings **879**, 1195 (2007).

[12] J. Feng *et al*., Applied Physics Letters **96**, 134102 (2010).

[13] M. Bonn *et al*., Physical Review B **61**, 1101 (2000).

[14] J. Hohlfeld *et al*., Chemical Physics **251**, 237 (2000).

[15] Detailed study of FDI measurments for the laser heated foils will be presented in a separate paper.

[16] M. Grioni *et al*., Physical Review B **39**, 1541 (1989).

[17] D. Coster, and R. D. L. Kronig, Physica **2**, 13 (1935).

[18] G. Paolo, and et al., Journal of Physics: Condensed Matter **21**, 395502 (2009).

[19] D. Prendergast, and G. Galli, Physical Review Letters **96**, 215502 (2006).

[20] D. Prendergast, and S. G. Louie, Physical Review B **80**, 235126 (2009).

[21] R. D. Leapman, and L. A. Grunes, Physical Review Letters **45**, 397 (1980).

[22] J. E. M¸ller, O. Jepsen, and J. W. Wilkins, Solid State Communications **42**, 365 (1982).

[23] W. S. Fann *et al*., Physical Review Letters **68**, 2834 (1992).

[24] V. P. Zhukov, and E. V. Chulkov, Physics Uspekhi **52**, 105 (2009).

[25] S. I. Anisimov, B. L. Kapeliovich, and T. L. Perel'man, Sov. Phys. JETP **39**, 375 (1974).

[26] H. E. Elsayed-Ali *et al*., Physical Review Letters **58**, 1212 (1987).

[27] Z. Lin, L. V. Zhigilei, and V. Celli, Physical Review B **77**, 075133 (2008).

**Figures & Captions**

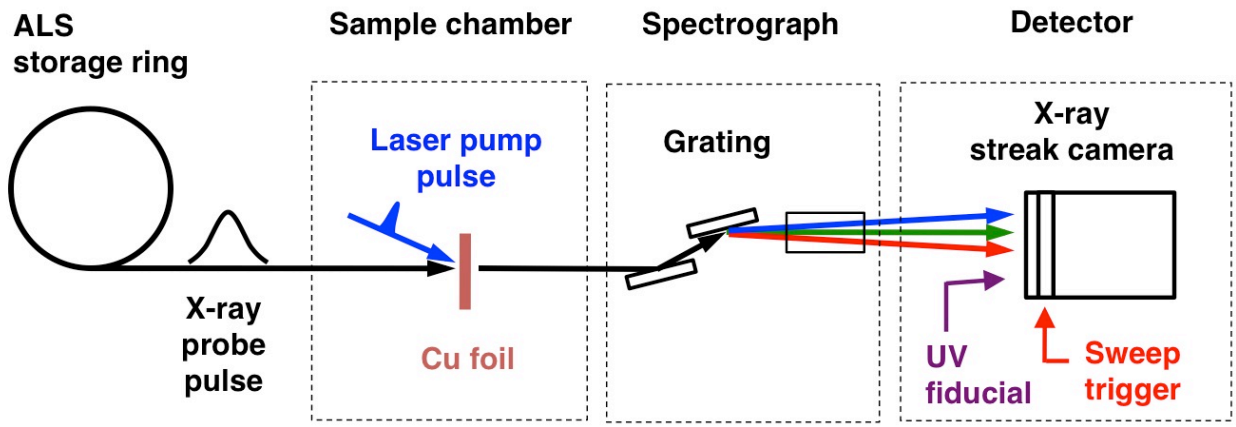


Fig 1. Schematic diagram of the experiment at ALS beamline 6.0.2. X-rays pass in transmission through the copper foil, are then dispersed by the grating spectrograph and finally detected by the x-ray streak camera.

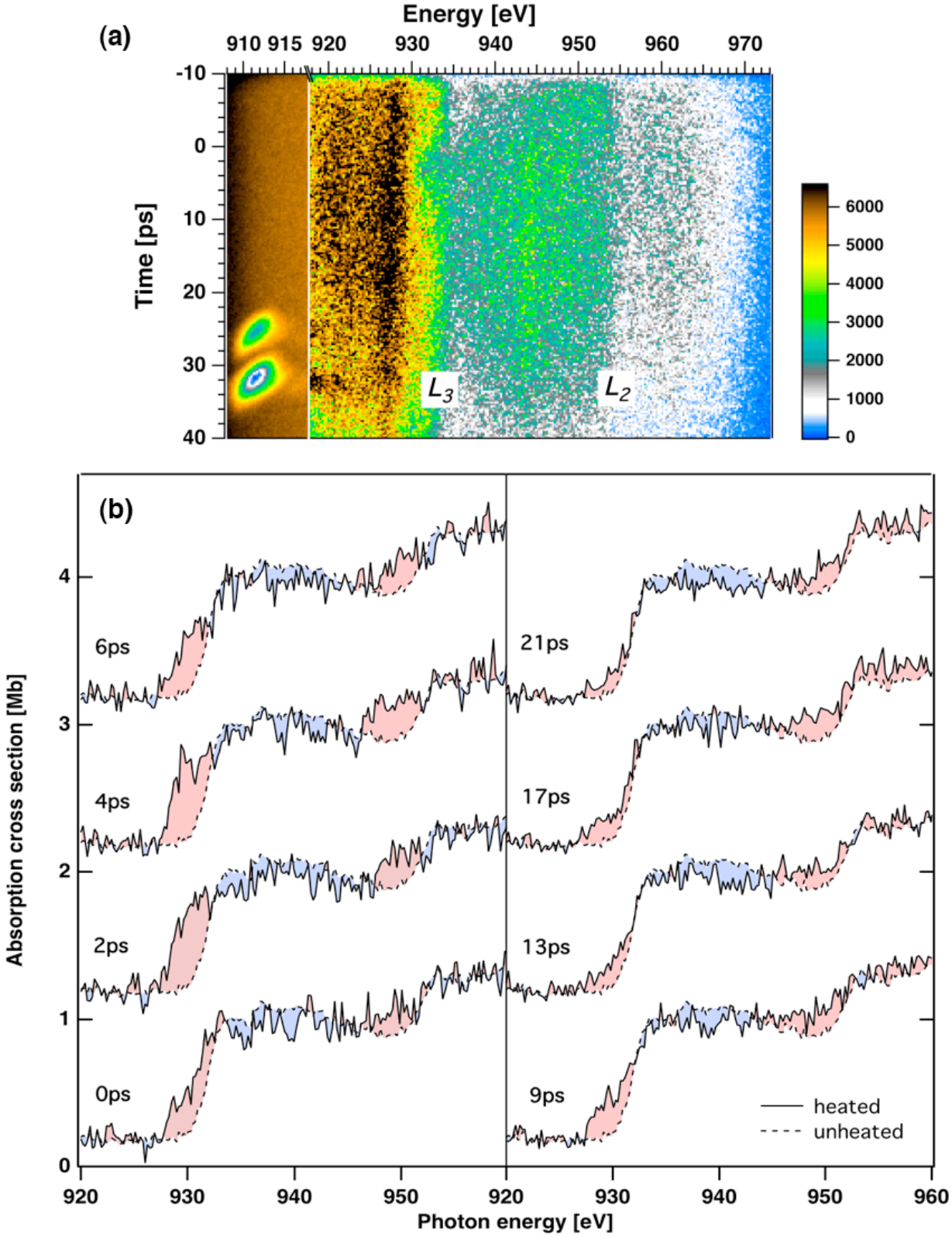
(a)
Energy [eV]
910 915 920 930 940 950 960 970
-10 0 10 20 30 40
Time [ps]
$L_3$
$L_2$
6000 5000 4000 3000 2000 1000 0
(b)
Absorption cross section [Mb]
0 1 2 3 4
6ps
4ps
2ps
0ps
21ps
17ps
13ps
9ps
heated
unheated
920 930 940 950 920 930 940 950 960
Photon energy [eV]

Fig 2. (a) An average x-ray streak camera image of the transmitted x-ray pulse through laser-excited copper showing time on the vertical axis and photon energy on the horizontal axis. The laser pulse at $t = 0$ causes a decreased transmission below both $L_3$ and $L_2$ edges. The two spots on the left side are UV time fiducials. To better view of the UV pulses, a different color scale is used for the left side of image. (b) The x-ray absorption spectra of warm dense copper at selected times (solid curves). Spectra are displayed with an offset of +1 along the *y*-axis between time steps. For comparison, the room temperature XAS of Cu is also shown as the dotted curves.

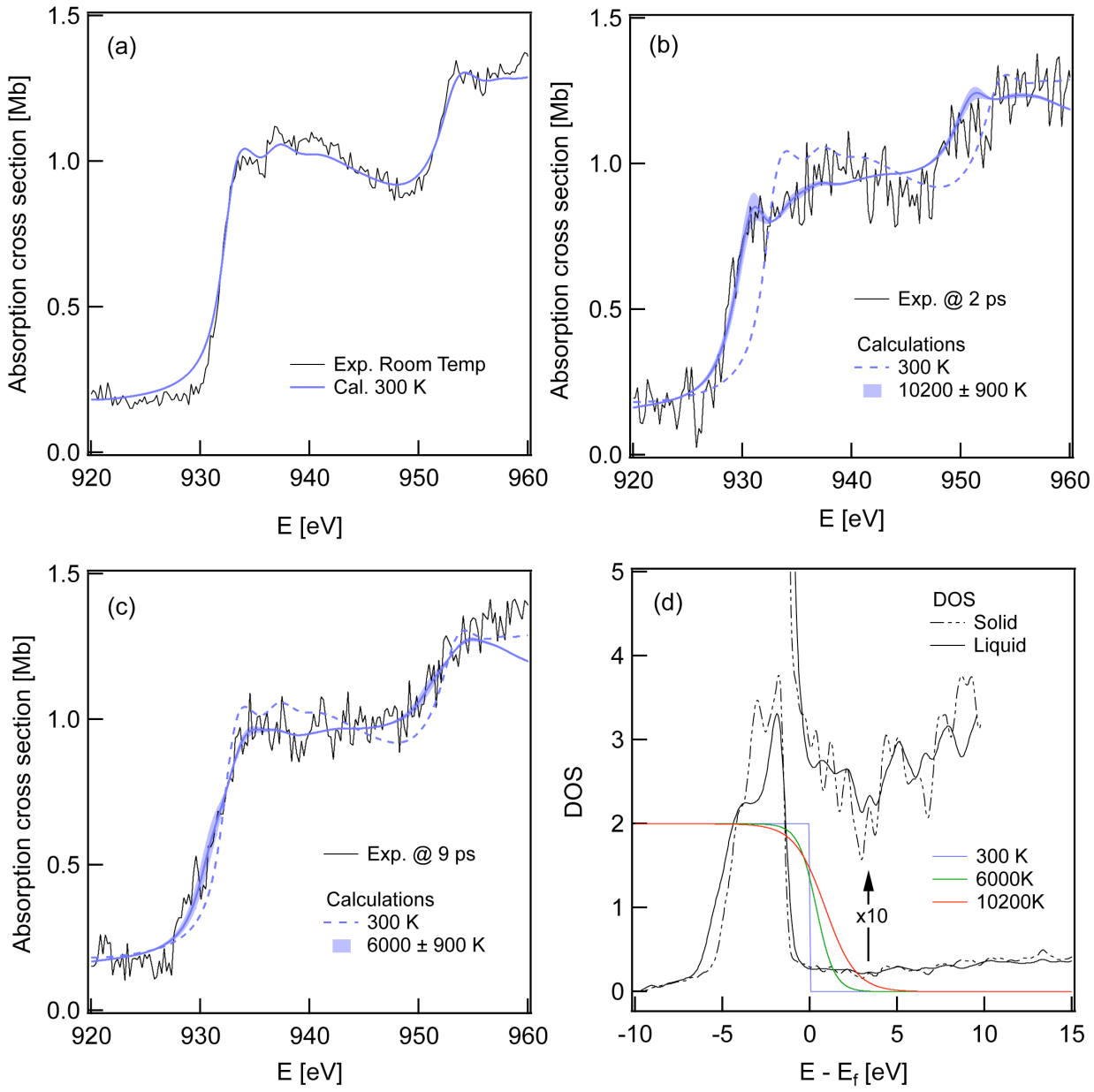


Fig 3. Comparisons of measured and calculated XAS for (a) the ambient state of copper and (b,c) the WDM states at selected times. Experimental data are shown as black curves and calculations at the given temperatures as blue curves. The shaded areas represent the spectra at a high and lower temperature. (d) The density of states of solid (dotted line) and liquid (solid line) copper

and the electron distributions at several temperatures used in modeling the time-dependence of the electronic temperature.

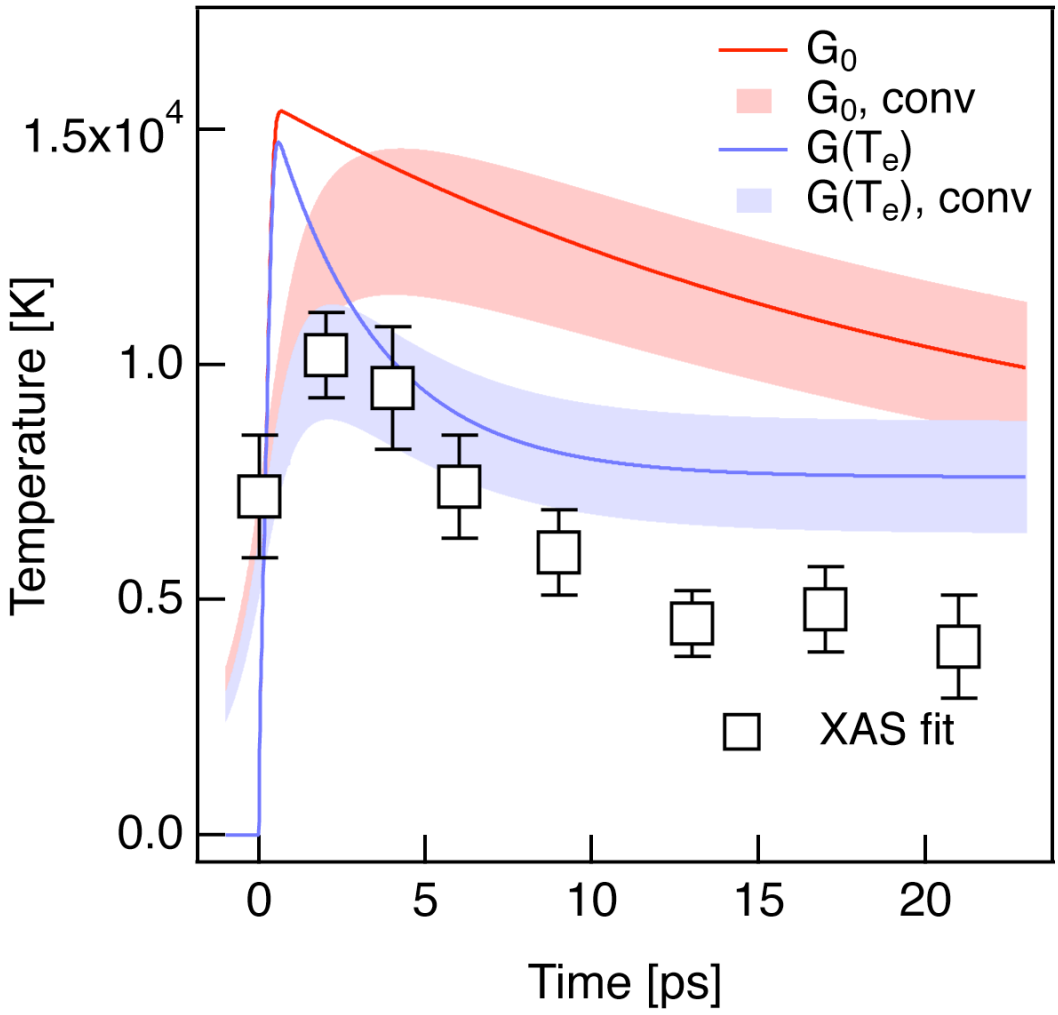


Fig 4. The temporal evolution of the electron temperature. Experimental-derived values of the electron temperature are shown as squares. For $G_0$ (red) and $G(T_e)$ (blue), solid lines are the electron temperatures calculated by the two temperature model with $E_d$ = 3.6 MJ/kg. The shaded areas represent TTM calculations combined with the experimental accuracies in the $E_d$ as well as the convolution with a detector response.